# Chalky versus foliated: a discriminant immunogold labelling of shell microstructures in the edible oyster Crassostrea gigas

Vincent Mouchi, Franck Lartaud, Nathalie Guichard, Françoise Immel, Marc de Rafélis, Cédric Broussard, Quentin G. Crowley, Frédéric Marin

# Chalky *versus* foliated: a discriminant immunogold labelling of shell microstructures in the edible oyster *Crassostrea gigas*

Vincent Mouchi[1,2*], Franck Lartaud[3], Nathalie Guichard[4,5], Françoise Immel[4,6], Marc de Rafélis[2,7], Cédric Broussard[8], Quentin G. Crowley[1], Frédéric Marin[4]

[1] Trinity College Dublin, School of Natural Sciences, Department of Geology, Dublin 2, Ireland

[2] Sorbonne Universités, UPMC Univ Paris 06, CNRS UMR 7193, ISTeP, F-75005, Paris, France (V.M : present address)

[3] Sorbonne Universités, UPMC Univ Paris 06, CNRS, Laboratoire d'Ecogéochimie des Environnements Benthiques, Observatoire Océanologique de Banyuls, F-66650 Banyuls/Mer, France

[4]UMR CNRS 6282 Biogéosciences, Université de Bourgogne – Franche Comté (UB-FC), Dijon, France

[5]UMR CNRS 6457 SUBATECH, La Chantrerie, Nantes, France (N.G : present address)

[6]UMR CNRS 5200 laboratoire de Biogenèse Membranaire, Université Bordeaux Segalen, Villenave d'Ornon, France (F.I : present address)

[7]UMR CNRS 5563 Géosciences Environnements Toulouse (GET), Université de Toulouse III Paul Sabatier, Toulouse, France (MdR : present address)

[8]UMR CNRS 8104 INSERM U1016 - Institut Cochin, Université Paris Descartes, Paris, France

[*] To whom correspondence should be addressed

**Key-words**

Crassostrea gigas; oyster shell; biomineralization; shell matrix extraction; polyclonal antibody; immunolocalization; in vitro crystallization; microstructures.

**Abstract**

Mollusc shells are organic-inorganic biocomposites, arranged in a limited number of superimposed calcified layers that generally exhibit very different organization of their crystallites. Because of their attractive mechanical and crystallographic properties, these shell layers have been the focus of several physical and biochemical characterizations. In particular, recent proteomic data obtained from individual layers suggest that their protein contents are different. However, the direct visual evidence that some macromolecular components are layer-specific is rather tenuous. This paper is based on a non-conventional immunogold labelling approach to localize proteins in the shell of the edible oyster *Crassostrea gigas*. The shell microstructure of this model organism is predominantly composed of foliated calcite, interspersed by discontinuous pockets of 'chalky layers', a porous microstructure typical of bivalves of the ostreid family. By developing a polyclonal antibody (in two rats) elicited against a proteinaceous shell fraction, we obtained differential staining of the two microstructures. We assert that our labelling is microstructure-discriminant. The difference in labelling of the two shell microstructures suggests either that they are formed by a variation of the secretory repertoire of the shell-forming cells of the calcifying mantle epithelium or that the chalky layer may be formed via a completely different mechanism. Our results allow a first glimpse on the subtle regulatory mechanisms that drive the process of chalky and foliated layers deposition.

## Introduction

To protect their soft body, most molluscs secrete an external rigid exoskeleton, the shell. The shell is an inorganic-organic biocomposite, predominantly made of calcium carbonate, with a minor fraction of occluded organics, about 1% of the shell weight (Marin et al. 2012). This fraction, a mixture of proteins, glycoproteins and polysaccharides, collectively described as the shell matrix, is the main regulator of mineral deposition (Weiner and Traub 1984; Lowenstam and Weiner 1989; Simkiss and Wilbur 1989). During calcification, the shell matrix is secreted by the calcifying mantle epithelium, together with inorganic precursor ions including calcium, bicarbonate and minor elements such as magnesium and strontium (Marin et al. 2012). All of these ingredients interact together at the interface between the mantle tissue and the growing shell and self-assemble to form crystalline architectures that are exquisitely crafted (Carter 1990).

Because of their mechanical properties, marine mollusc shells are often taken as a model for biomineralization studies (Addadi et al. 2006) and, more generally, as an inexhaustible source of inspiration for generating organic-inorganic composites with tailored mechanical properties and shapes (Cranford and Buehler 2010). In addition to these biotechnological applications, mollusc shells are studied for their capacity to record with high reliability the variations of physicochemical parameters of seawater (Rhoads and Lutz 1980). In recent years, this second aspect has become more pressing in the context of concern over global changes, in particular, of ocean acidification (Orr et al. 2005).

Oysters are excellent mollusc models for such environmental studies. Oysters are marine and brackish bivalves of the pteriomorphid subclass with a number of advantages; firstly, they are ubiquitous, occurring all over the world oceans and seas with the exception of polar regions, allowing comparisons at the global scale. Secondly, they withstand different

salinities (Bricteux-Grégoire et al. 1964) and different water depths (van Rooij et al. 2010), and can consequently be used as markers in different environments. Thirdly, their shell is entirely made of low magnesium calcite – with the exception the restricted myostracal layer that is aragonitic (Taylor et al. 1969) – and thus, resists diagenetic transformations better than most aragonite and high magnesium calcite shells (Ahr 2008). Oysters exhibit a large stratigraphical range that covers the last two hundred million years of the history of Earth (Marquez-Aliaga et al. 2005), allowing extensive palaeoenvironmental reconstruction studies at different geological periods. Finally, their shell is thick, *i.e.*, ideal from a practical viewpoint for measuring with high accuracy environmental proxies along transects, in both recent (Lartaud et al. 2010a; Mouchi et al. 2013) and fossil (Bougeois et al. 2014, 2016) specimens.

Our study focuses on one member of the ostreid family, *Crassostrea gigas*, the edible cupped oyster, also called the giant Pacific oyster, and a model of economic interest (Gosling 2003). *Crassostrea gigas* can withstand huge environmental variations, including alternation of emersion/immersion, drastic change in salinity and rapid increase/decrease of temperature (Lartaud et al. 2010a). *Crassostrea gigas* shell allows a very precise temporal calibration, independently from the shell microstructures (Lartaud et al. 2010b). The shell of *C. gigas* exhibits two main textures: the foliated and chalky microstructures. Foliated calcite can be described as "*a laminar structure consisting of parallel calcitic laths arranged in sheet dipping at the same angle and in the same general direction over a large portion of the depositional surface"* (Carter and Clark II, 1985). The chalky microstructure is typical of Ostreidae and predominantly found in this bivalve family. It forms discontinuous, lenticular bodies that are intercalated between the folia. Numerous studies have reported different putative mechanisms for the formation of chalky layers (Orton and Amirthalingam 1927; Korringa 1951; Palmer and Carriker 1979; Vermeij 2014). So far, no consensus emerged.

In the present paper, we used an immunolabelling approach – complementary to that developed by one of us (F. L.) with manganese – to label the shell of *C. gigas*. To this end, we employed the following strategy: the shell matrix was extracted, characterized on monodimensional electrophoretic gels, and one fraction was further purified by preparative SDS-PAGE before being analyzed by proteomics, and tested for its ability to interact with the *in vitro* precipitation of calcium carbonate. This protein fraction was subsequently used to elicit polyclonal antibodies, which, after accurate testing, allowed immunolabelling of the shell. This labelling is microstructure-discriminant. The difference in labelling of the two shell microstructures suggests that their elaboration rests upon a variation of the secretory repertoire of the shell-forming cells of the calcifying mantle epithelium.

## Materials and methods

### Sample preparation

Fresh oysters were collected live in Dublin area, Ireland. For specimens used for matrix extraction, shells were emptied, the muscle scar scrupulously cleaned, and the outer surface of the shells mechanically abraded with a rotary tool (Dremel) to remove all epibionts that could act as a source of contaminant material. Whole shells were then chemically cleaned in dilute sodium hypochlorite (0.26 % active chlorine) for 48 h and rinsed thoroughly in deionized water several times. Shells were mechanically crushed in small fragments (4-5 mm) that were placed in sodium hypochlorite (0.26 % active chlorine) for 24 h. They were rinsed several times in Milli-Q water, dried at 37 °C and powdered using a mortar grinder (Pulverisette 2, Fritsch, Idar-Oberstein, Germany). The powder was sieved to select particles with a grain size below 200 µm.

For immunogold localization, additional shells were taken from the collection of the Institut des Sciences de la Terre de Paris (ISTeP, UPMC). These specimens had been previously bred for two years at Baie des Veys (Normandy, France) according to a published paper (Lartaud et al. 2010b). The shells were emptied and chemically cleaned with hydrogen peroxide (6 %) for 6 h followed by 0.15 N nitric acid for 20 min and washed in demineralized water. The hinge areas were cut from the shells, and hinge sections were glued with epoxy to glass plates and sawed to a thickness ranging from 500 µm to 1 mm, in order to visualize the chalky and foliated shell microstructures.

Shell matrix extraction

The protocol used for matrix extraction was, with slight differences, used in previous papers (Osuna-Mascaró et al. 2014; Kanold et al. 2015): 25.08 g of shell powder was suspended in 100 mL of Milli-Q water under constant stirring, at 4 °C. The powder was slowly decalcified overnight with cold dilute acetic acid (10 %vol.vol$^{-1}$), with additions every 5 s (100 µl) using an electronic burette (Titronic Universal, Schott, Mainz, Germany). At the end of the decalcification, the resulting solution (>1 L) was centrifuged for 15 min at 3900 *g*. The supernatant containing the acid-soluble matrix (ASM) was separated from the pellet of the acid-insoluble matrix (AIM). The AIM was scrupulously rinsed by a series of resuspensions in milli-Q water/centrifugation (5 cycles). Each time, the resulting supernatants were added to the ASM. The AIM was finally lyophilized and weighed. The ASM was filtered on a Nalgene device with a 5 µm filter then its volume was reduced by ultrafiltration using a 400 mL Amicon cell with a 10 kDa cutoff membrane. At the end of the concentration process (final volume around 15 mL), the solution was dialyzed at 4 °C in a Spectra/Por tube (cutoff 1000 Da) against milli-Q water, with 5 water changes in 4 days. The solution was lyophilized

overnight, and the resulting pellet, weighed. A second extraction was performed in similar conditions, with 30.03 g of shell powder.

Shell matrix analysis on 1D gel electrophoresis

ASM and AIM fractions were both analyzed by conventional mono-dimensional electrophoresis on 12 % polyacrylamide mini gels (Mini-Protean III, Bio-Rad, Hercules, CA, USA) following the manufacturer's instructions. Both matrices were resuspended in Laemmli sample buffer (LSB) containing ß-mercaptoethanol, and denatured by heating at 100 °C for 10 min. The solutions were cooled down on ice then centrifuged for 2 min. A fraction of the AIM was further solubilized by the Laemmli buffer and this soluble fraction was referred to as the LS-AIM (Laemmli-Soluble AIM). The proteins were fractionated on the gel for 15 min at 100 V, and then for about one hour at 150 V. The gel was stained with silver nitrate according to the protocol of Morrissey (1981), with the modification that the colour development was stopped with 3 M citric acid.

Protein extraction and fraction purification

Following the separation of the proteins in gel, one of the most abundant proteins was purified on a large scale, according to the procedure described in Marin et al. (2001) and Marin (2003): 2 mL of Milli-Q and 2 mL of LSB (2x) were admixed to 124 mg of extracted AIM and the preparation was denatured by heating at 100 °C for 10 min. Fractionation of the proteins of the LS-AIM was performed at 180-200 V for the stacking and 300 V for the running in a 12 % acrylamide preparative gel was cast in a Bio-Rad model 491 Prep Cell. The complete LS-AIM extract was eluted from the gel in about 13 hours and collected in 80 tubes (5 ml per tube, flow rate of elution: 0.5 ml/min). All 80 fractions were tested with dot-blot using a Bio-Rad Bio-Dot on a PVDF membrane. The membrane was subsequently treated

with polyclonal antibodies elicited against calprismin, a 37 kDa protein from the prismatic layer of the bivalve *Pinna nobilis* (Marin et al. 2005). This antibody presented a strong cross-reactivity with the shell matrix of *C. gigas* in preliminary tests and recognized epitopes of relatively abundant protein of the AIM in Western-Blot (results not shown here). Two consecutive fractions presenting such strong reaction were pooled, and the resulting solution dialyzed (Spectra/Por tube, 4 °C) and lyophilized. The purity of this extract, referred as F21-22, was tested on a 12 % polyacrylamide gel, similarly to what described above.

Proteomics on the purified fraction

The identification of the protein content of F21-22 was performed via a proteomic approach, according to an in-gel digestion, as previously described (Kanold et al. 2015). The fraction was denatured and run on a precast 12 % acrylamide mini-protean TGX gel (Bio-Rad). The gel was fixed overnight (colloidal Coomassie blue), then washed in Milli-Q water, and a band manually sliced near 30 kDa. The slice was cut into cubes, which were subsequently placed in an Eppendorf tube. Then, in-gel digestion was carried out with trypsin, according to a published procedure with minor adjustments (Shevchenko et al. 2001): the sample was destained twice with a mixture of 100 mM ammonium bicarbonate (ABC) and 50 % (vol.vol$^{-1}$) acetonitrile (ACN) for 45 min at 22 °C and then dehydrated using 100 % ACN for 15 min, before being reduced with 25 mM ABC containing 10 mM DTT for 1 h at 60 °C and alkylated with 55 mM iodoacetamide in 25 mM ABC for 30 min in the dark at 22 °C. Gel pieces were washed twice with 25 mM ABC and dehydrated (twice, 15 min) and dried (10 min) with 100 % ACN. Gel cubes were incubated with sequencing grade modified trypsin (Promega, USA; 12.5 ng.µl$^{-1}$ in 40 mM ABC with 10 % ACN, pH 8.0) overnight at 40 °C. After digestion, peptides were washed with 25 mM ABC, dehydrated with 100 % ACN and

extracted twice with a mixture of 50 % ACN–5 % formic acid (FA). Extracts were dried using a vacuum centrifuge Concentrator plus (Eppendorf).

For MS and MS/MS ORBITRAP, analyses were performed using an Ultimate 3000 Rapid Separation Liquid Chromatographic (RSLC) system (Thermo Fisher Scientific) online with a hybrid LTQ-Orbitrap-Velos mass spectrometer (Thermo Fisher Scientific). Briefly, peptides were dissolved in 4 µL of 10 % ACN-0.1 % FA. Then peptides were loaded and washed on a $C_{18}$ reverse phase precolumn (3 µm particle size, 100 Å pore size, 150 µm i. d., 1 cm length). The loading buffer contained 98 % $H_2O$, 2 % ACN and 0.1 % TFA. Peptides were then separated on a $C_{18}$ reverse phase resin (2 µm particle size, 100 Å pore size, 75 µm i. d., 15 cm length) with a 1 h gradient from 100 % A (0.1 % FA and 100 % $H_2O$) to 50 % B (80 % ACN, 0.085 % FA and 20 % $H_2O$).

The Linear Trap Quadrupole Orbitrap mass spectrometer acquired data throughout the elution process and operated in a data dependent scheme with full MS scans acquired with the Orbitrap, followed by up to 20 LTQ MS/MS CID spectra on the most abundant ions detected in the MS scan. Mass spectrometer settings were: full MS (AGC: $1 \times 10^6$, resolution: $6 \times 10^4$, m/z range 400–2000, maximum ion injection time: 500 ms) and MS/MS (AGC: $5 \times 10^3$, maximum injection time: 20 ms, minimum signal threshold: 500, isolation width: 2 Da, dynamic exclusion time setting: 30 s). The fragmentation was permitted for precursors with a charge state of 2, 3, 4 and above. For the spectral processing, the software used to generate .mgf files was Proteome discoverer 1.3. The threshold of signal to noise for extraction values is 3. Database searches were carried out using Mascot version 2.4 (Matrix Science, London, UK) on “other metazoa” proteins (35,149,712 sequences) from the NCBInr databank containing 12,374,887,350 residues (January 2014) (www.ncbi.nlm.nih.gov/) and an in-house shell protein databank (762 sequences containing 220,545 residues). The search parameters were as follows: carbamidomethylation as a variable modification for cysteins, and oxidation

as a variable modification for methionines. Up to 1 missed tryptic cleavage was tolerated, and mass accuracy tolerance levels of 10 ppm for precursors and 0.45 Da for fragments were used for all tryptic mass searches. Positive identification was based on a Mascot score above the significance level (i.e. b5 %). The reported proteins were always those with the highest number of peptide matches.

Antibodies production, ELISA testing and Western blots

The fraction was used to produce polyclonal antibodies (Eurogentec, Seraing, Belgium) in two rats, SER323 and SER324, following a standard immunization procedure: the rats were injected (60 μg of antigens per injection) at day 0, then at days 14, 28, 56 and 132, and their blood was collected at day 0 (pre-immune serum, PPI), 38 (small bleed, PP), 66 (large bleed, GP) and 142 days (final bleed, SAB). The titers of the different antibody solutions were checked by conventional ELISA (Clark and Adams 1977; Thresh et al. 1977): in brief, the antigens were incubated in a Nunc Maxisorp 96 well microplate (200 ng per well, 90 min, 37 °C). After blocking step (0.5 % wt.vol$^{-1}$gelatin in TBS), the microplate was incubated 90 min. with the antibody solutions (PPI, PP, GP, SAB, diluted 1/100 to 1/200000), then with the secondary antibody (goat anti-rat, Sigma A 8438, diluted 30000 times). The microplate was thoroughly rinsed with TBS/Tween 20 (using a manual Nunc Immuno Wash 12 microplate washer) between antigen incubation and blocking and after the 1$^{st}$ and 2$^{nd}$ antibodies incubations. The microplate was revealed with the substrate solution, consisting of p-nitrophenylphosphate (5 mg tablet in 10 mL) dissolved in a water:diethanolamine solution (10:1), pH 9.8. After short incubation at 37°C, it was read with a multichannel spectrophotometer at 405 nm. We checked that the two pre-immune sera gave no reactivities and consequently used the different sera for further characterization.

Western blots (Towbin et al. 1979) were used to test the specificity of the antibodies against the matrix of the shell of *C. gigas*. Both LS-AIM and ASM were tested on 12 % polyacrylamide mini-gels. After migration, the proteins from the gels were electro-transferred on a PVFD membrane (Immobilon, Millipore) for 90 min at 100 V in a Bio-Rad Mini Trans-Blot module. The membrane was then blocked in a TBS solution containing 1 % gelatin for 30 minutes before placed in a TBS solution containing 1 % gelatin, 0.05 % Tween 20 and the antibodies diluted 1500 times. The membrane was incubated for 3 hours at 37 °C and then rinced several times in a TBS/Tween 20 solution. It was subsequently incubated 90 minutes in a TBS/Tween 20/gelatin solution containing secondary antibodies (goat-anti-rat, Sigma, ref. A8438) coupled with alkaline phosphatase, diluted 30,000 times. Finally, the membrane was rinced thoroughly (5 x 10 min) in TBS/Tween 20 and incubated for five minutes in the dark in CDP-Star (Sigma, ref. C0712) solution. The chemoluminescent signal was recorded by mounting the membrane between two write-on transparency sheets in a cassette and exposing it shortly to a X-OMAT Kodak film which was conventionally developed and fixed. In addition, the nitrocellulose membrane was stained with NBT/BCIP (Sigmafast tablets, Sigma, ref. B5655).

Specificity of the antibody responses to microstructures

In order to check the extent to which the antibodies could differentiate the matrix of the individual shell microstructures of *C. gigas*, we performed specific ELISA with extracts from the chalky and foliated layers as previously described (Marin et al. 1999). In brief, left valves were cut in half to expose the hinge region showing the two microstructures. The chalky and foliated microstructures were collected separately using a dental drill. 40 mg of each powder were dissolved overnight in 4 mL EDTA solution (10 %wt.vol$^{-1}$). After a short centrifugation (3900 *g*, 10 min), aliquots of the EDTA-extracts were directly incubated in 96-well

microplates (37°C, 90 min.). A conventional ELISA test, as described above, was performed with each of the sera (PP, GP, SAB) obtained from both rats. The microplate was read at 405 nm. PPI (pre-immune serum) was used as a negative control.

*In vitro* crystallization test

Both the ASM and the purified fraction of the AIM (F21-22) were tested for their capacity to influence the growth of calcium carbonate crystals, according to a procedure derived from that of Albeck et al. (1993). Briefly, calcite crystals were grown by the interaction between vapours of ammonium bicarbonate and $CaCl_2$ solution (10 mM) containing a small quantity of ASM or F21-22. The $CaCl_2$ solution (200 µL) with different quantities of matrix (from 0.3125 to 20 $\mu g.mL^{-1}$) was placed in the wells of a 16-well culture slide (Lab-Tek, Nunc). The cover of the slide was pierced to allow diffusion of ammonium bicarbonate vapours. The culture slide with its cover was sealed with Parafilm then placed at 4 °C in a 5 L closed desiccator containing crystals of ammonium bicarbonate for 72 h. Control scenarios of only $CaCl_2$ solution were tested in parallel. After incubation, the solution was carefully removed from each well using a blunt-ended needle connected to a vacuum system. The glassplate of the slide was dissociated from the well spare part and directly observed under a Hitachi TM1000 Tabletop microscope without carbon coating. This experiment was repeated four times to ensure homogeneity of the results.

Protein localization by immunogold by SEM

Small freshly fractured (<5 mm) fragments were placed in sodium hypochlorite solution to remove superficial contaminants. They were rinsed (milli-Q water), dried then slightly etched in EDTA solution (1 $\%wt.vol^{-1}$) for 3 min to expose antigenic determinants. For the cleaning and etching steps, ultrasonic baths were not used, to avoid fragmentation of the shell pieces.

The samples were then washed for 1 min in TBS before being blocked in filtered TBS/gelatin (0.5 %) solution (pH adjusted to 7.5 with dilute NaOH solution) for 30 min. The shell samples were subsequently incubated 3 h in TBS/Triton/gelatin containing the antibodies (GP and SAB) diluted 500 times. They were rinsed 5 times in TBS/Triton for 10 min and incubated 3 hours in TBS/Triton/gelatin (0.5 %) containing the secondary antibody (goat-anti-rat, 5 nm gold conjugate, BBI ref. EM.GTMA5, dilution 1/100). They were thoroughly washed in TBS/Triton then in water and slightly dried by capillarity. Fragments were finally silver-enhanced (BBI ref. SEKL.15) for 15 minutes before being rinsed in Milli-Q and dried at 37 °C. Several negative controls were performed, by using PPI, or by replacing the antibodies ($1^{st}$ and/or $2^{nd}$) by TBS/Triton/gelatin. Observations were performed on the Hitachi TM1000 Tabletop microscope without carbon coating. The test was repeated three times.

## Results

Microstructures of the shell of *Crassostrea gigas*

As shown by Fig. 1, the shell of *C. gigas* is composed predominantly of two microstructures: the main one is foliated calcite, classically described by Taylor et al. (1969), Runnegar (1984) and Carter and Clark II (1985), and consisting of parallel calcitic laths arranged in sheets; the chalky layer, discontinuous, forming lenses in the hinge region (Fig. 1a) and intercalating thin layers in the other parts of the shell. From a microstructural viewpoint, chalky layers appear far more porous and made of a framework of blade-shaped (Margolis and Carver 1974) crystals that develop more or less perpendicularly to the mineral depositional plan. The blades are linked with each other by leaflets that branch at different angles (Fig. 1b), leaving a large amount of empty space. Between the framework, the space is filled by tangled crystals. In

addition to the foliated and chalky microstructures, a thin prismatic calcitic layer is observed, constituting the outermost part of the shell (not shown in Fig. 1).

Shell matrix extraction and characterization on mini-gels

Similar amounts of ASM and AIM were obtained from the different fractions. From the first batch (25.08 g shell powder), we quantified 11.25 mg of ASM and 116.84 mg of AIM, representing 0.045 % and 0.465 % of dry weight of shell powder, respectively, representing together about half a percent of organics. The AIM/ASM ratio is about 10. When proteins were fractionated on a monodimensional gel and stained with silver, the profile (Fig. 2a) shows few proteins on each of the fractions distinct from some smearing material. ASM (Fig. 2a lane 1) contains 3 main proteinaceous components at approximately 45, 27 kDa and 12 kDa. The electrophoretic pattern of LS-AIM (Fig. 2a lane 2) exhibits similarities with that of ASM, since these 3 proteins are present, in addition to three other diffuse proteinaceous components at approximately 60, 34 and 22 kDa. In both extracts, the 45 kDa proteinaceous component is negatively stained. In the ASM, the upper part of the gel (above 130 kDa) and the zone between 17 and 30 kDa present also this particularity.

Protein purification and testing of antibodies

The whole LS-AIM was fractionated on a preparative gel electrophoresis, and the fractions were dot-blotted. The fraction of interest was eluted in tubes 21-22, and further processed, including extensive dialysis and freeze-drying (Fig 2b). It was referred as F21-22 (Fig. 2c). After extensive dialysis and freeze-drying, 2.13 mg of purified protein was obtained from 30 g of shell powder. The fraction, when tested on a mini-gel, is revealed as a thick proteinaceous component around 27 kDa (Fig. 2d). After production of polyclonal antibodies in two rats (SER323 and SER324), titers from the PPI, PP, GP and SAB bleeds were

348 determined in ELISA (Fig. 3). Pre-immune bleeds from both rats show no reaction to the
349 targeted fraction. For rat SER323, the final titer (about 1:1500) is almost reached after the
350 first injection (PP bleeding), and the differences of immunological reactivity between the
351 successive bleeding are minimal. For rat SER324, we observe a progressive increase of the
352 titer, in correlation with the successive immunizations. In this case, titers are 1:100, 1:500 and
353 1:1000 for PP, GP and SAB, respectively.
354
355
356 Western-blots of shell extracts with the anti-F21-22 antibody
357 The results of the Western blot of the shell extracts with the anti-F21-22 antibody from the
358 rats SER323 and SER324 are shown on Fig. 4. For each of them, we present the data obtained
359 with PPI (negative control, left), 2$^{nd}$ bleed (GP, center) and final bleed (SAB, right). For the
360 clarity of the results, we only illustrate the Western blots obtained after the chemical staining
361 of the membrane with NBT/BCIP. Entirely superimposable results, although more blurred,
362 were obtained with the chemoluminescent CDP-Star. None of the two PPIs react with the
363 shell extracts, ASM or LS-AIM. When tested on F21-22, the antibodies from the two rats
364 successfully recognize this fraction, giving a high intensity signal. Although the antibodies
365 were elicited against a discrete molecular weight fraction, their response against the whole
366 ASM and LS-AIM encompasses a broad range of molecular weights, from above 170 kDa to
367 about 10 kDa. For rat SER323 (Fig. 4a), we notice that the antibody allows visualizing
368 proteins that cannot be discriminated on the silver-stained gel, in particular proteins of high
369 molecular weights around 72, 130 and above 170 kDa. These proteinaceous components are
370 observed both for ASM and LS-AIM from GP and SAB (Fig. 4a). Other proteins do cross-
371 react around 50 and 40 kDa in the same lanes. For rat SER324, we obtain a different pattern,
372 since the corresponding antibody stains preferentially the smear than the discrete proteins. In

the ASM (Fig. 4b, SAB), the F21-22 fraction is well marked. For both rats, the staining of LS-AIM is more pronounced than that of ASM. Signals given by GP bleeds are weaker than those of SAB bleeds, particularly for rat SER324. This finding is congruent with the ELISA results.

Proteomics on the F21-22 fraction

The proteomic investigations, as summarized in Table 1, yielded a series of peptides that match with three proteins or protein families of *C. gigas* that are, respectively: Gigasin-6, and two of its isoforms Gigasin-6 X1 and Gigasin-6 X2; two nacrein-like proteins; a cell death abnormality protein 1-like. Gigasin and its two isoforms X1 and X2 were identified by an identical set of three different peptides. Each of the two nacrein-like proteins were also identified by three peptides, two of which being identical in the two proteins, while the third differed only by one amino acid residue (D or E). Two peptides – among which a 23 amino acid residues long hydrophobic peptide - could assign the cell death abnormality protein 1-like. The positions of these peptides along the different protein sequences are visualized in the supplementary Fig. 1. Additional *in silico* investigations in less stringent conditions (lower threshold, not shown in Table 1) generated six peptides – all located in the N-terminal region of the protein - that match with a transcription termination/antitermination protein NusA-like from the Mediterranean Fruit fly *Ceratitis capitata* (gi|498978467). The significance of these additional hits is not understood.

*In vitro* crystallization in the presence of ASM and of F21-22

Results of the *in vitro* crystallization assay with fraction F21-22 and with ASM are shown on Fig. 5. The control scenario with no protein (Fig. 5a) produces single crystals that exhibit the typical rhombohedral morphologies of calcite. Effects are markedly different between the two

extracts. At low concentration (0.31 µg.mL$^{-1}$), ASM exhibits a pronounced effect on the crystal shape, with the formation of polycrystalline aggregates (Fig. 5e). At the same concentration (Fig. 5b), fraction F21-22 exerts almost no effect on the crystal morphologies. At 5 µg/mL, the effect induced by ASM is strong (Fig. 5f) while it is limited with fraction F21-22 (Fig. 5c). At high concentration (20 µg.mL$^{-1}$), ASM induces only polycrystalline aggregates that are completely rounded: some of the crystals are overgrown on their edges (Fig. 5g); with F21-22, we notice the formation of polycrystalline aggregates, similar to that produced at low concentration of ASM. In summary, the effect of the ASM is more pronounced than that of the fraction F21-22, at equivalent concentrations.

Response of the antibodies to microstructures

When tested by ELISA on extracts of the chalky and foliated microstructures, the antibodies of the two rats give different responses, illustrated by the histograms of Fig. 6: although the two series of antibodies cross-react with EDTA-extracts of both layers, SER323 antibodies recognize preferentially the one of the chalky layer (Fig. 6a), while SER324 antibodies give a stronger signal with the one of the foliated layer (Fig. 6b). For each of them, the most important differential response between the chalky and the foliated extracts is recorded with the GP bleeding, for which the reactivity ratio is about 2. The differences are attenuated with the final bleed (SAB).

Immunogold staining of *C. gigas* shell microstructures

Results of the immunolocalization based on the antibody elicited against F21-22 fraction are indicated on Fig. 7. Sections (Fig. 7a, b) and fresh fracture surfaces (Fig. 7c-h) are illustrated and give congruent results. We observe a double phenomenon: firstly, a differential immunolocalization of the epitopes recognized by anti-F21-22 on the chalky and on the

foliated microstructures, respectively; secondly, different responses, due to the rats that generated the antibodies. While rat SER323 generated antibodies that recognize preferentially the chalky layer, rat SER324 produced antibodies that mainly target epitopes of the foliated layer and only few structures of the chalky layer.

The antibodies produced by SER323 and used on the fresh fracture surfaces (Fig 7c-d) mark the edges of the sheets composing the foliated structure. It is worth noticing that the surfaces of the sheets (parallel to the growth plane) are never stained. The SER323 antibodies stain the chalky layer more or less uniformly. SER324 antibodies produce intense staining of the foliated layer, together with a staining located specifically on a 'chalky scaffold' perpendicular to the growth plane (Fig. 7e-h). SER324 antibodies stain none of the other structures present in the chalky layer.

## Discussion

We have developed a non-conventional strategy for marking the shell of the edible cupped oyster *Crassostrea gigas*, one of the few bivalve models for which genomic data are available (Zhang et al. 2012). To this end, we have extracted the shell matrix, for characterization and selection of an immunogenic protein fraction, which is a potential appropriate marker of shell calcification. The resulting polyclonal antibody preparation has allowed us to perform differential immunogold staining of the shell microstructure.

The extracted matrix exhibits similar features to those extracted from other mollusc shells. Indeed, the proportions of ASM and AIM fractions to the dry weight of the shell enters the range observed for other bivalves (Marin et al. 2012). In particular, a 1/10 ratio between ASM and AIM quantified in this study is frequently found for the matrices of several nacro-

prismatic bivalves (Marie et al. 2007). Our ASM:AIM values are also comparable to that of Marie et al. (2011) who extracted the equivalent of 0.4 % of AIM and 0.05 % of ASM from the same species. When fractionated using electrophoresis, the matrix – both ASM and LS-AIM – is constituted of a mixture of polydisperse ('smear') and few discrete macromolecules, *i.e.*, proteins, and the two fractions exhibit similar electrophoresis patterns. Although not tested in the present study, they may have overlapping protein compositions: our former proteomic investigations on different bivalve models demonstrated such similarities in protein compositions (Marie et al. 2009, 2010). This suggests that part of the AIM fraction may result from a polymerization/cross-linking of the ASM (Samata et al. 2008). Finally, we verified that the ASM interacted – in a dose-dependent manner – with the *in vitro* crystallization of calcium carbonate.

This overall characterization of the shell matrix served as a basis for further purification of an immunogenic protein fraction that was subsequently used for eliciting polyclonal antibodies. The purified fraction exerted an effect on the *in vitro* formation of calcium carbonate, but this effect was reduced in comparison to the one recorded with the whole ASM, suggesting synergistic effects of the different constituents of the ASM. When tested for proteomics, the fraction generated a short set of peptides that correspond to three proteins or protein families identified in the genome of *C. gigas*. The first protein family is that of gigasin-6 and its isoforms. Gigasin-6 is a 34 kDa (302 AA residue-long), leucine-rich protein with a basic p*I*, which exhibits a C beta-lactamase-like domain, a domain that catalyses the opening and hydrolysis of the beta-lactamine ring of this class of antibiotics, which include penicillins and cephalosporins. Interestingly, gigasin-6 was one of the eight proteins that were identified by us in a former study on the shell constituents of *C. gigas* (Marie et al. 2011). Its function in calcification remains unknown. The second family corresponds to nacrein-like proteins. Nacrein was initially identified and characterized in the

shell of the Japanese pearl oyster *Pinctada fucata* (Miyamoto et al. 1996). Then, several members, referred to as nacrein-like proteins, were identified in numerous molluscs and other metazoans. Nacreins and nacrein-like proteins exhibit similar primary structure: they possess a carbonic anhydrase (CA) domain, the function of which is to reversibly catalyse the conversion of carbon dioxide into bicarbonate (Le Roy et al. 2014). In addition, they exhibit a supernumerary domain, which is, in the present case, of the aspartic acid-rich type. Such a domain is likely to be involved in mineral interaction (Le Roy et al. 2014). Finally, our proteomic analysis identified a third member, a cell death abnormality protein 1-like belonging to a group of conserved proteins involved in cell apoptosis. This protein has a theoretical molecular weight of 28 kDa and is enriched in arginine and cysteine (about 12 % each) and in glycine and proline (about 9 %). The reason of the presence of such a protein in our shell fraction is obscure, and we cannot exclude the possibility that it was recruited for calcification to display a completely different function than that related to apoptosis. Note that this protein was not identified in our former proteomic study (Marie et al. 2011) on the whole matrix: we observed indeed that performing proteomics on electrophoresis fractions improve proteomics signals and allows the identification of rare proteins that are currently overshadowed by abundant ones in the mixture of the skeletal matrix macromolecules (Kanold et al. 2015). One intriguing aspect of our proteomic analysis is that the two nacrein-like proteins exhibit a molecular weight higher than that expected from the electrophoresis fraction (26-30 kDa), while that of the cell death abnormality protein 1-like and of gigasin-6 fit approximately into this molecular weight range. This calls for two explanations that are not mutually exclusive: on one hand, we cannot rule out that nacrein-like proteins may have an anomalous migration due in particular to their acidic supernumerary domain and that they migrate ‘faster’ than expected; on the other hand, it is possible that these proteins may partly

497 degrade in the shell when occluded; consequently, what we detect by proteomics are simply
498 degradation products that co-elute with gigasin-6/cell death abnormality protein 1-like.
499 The purified fraction was used to generate polyclonal antibodies in two rats.
500 Interestingly, although the antibody batches (SER323 and SER324) cross-react with several
501 discrete and non-discrete macromolecules of the ASM and LS-AIM fractions, as shown by
502 Western blots, both gave different cross-reactivities, in term of specificity. Such a variation
503 can be expected, as two animals immunized with the same antigens in identical conditions do
504 not react similarly (Hanly et al. 1995). In addition, our antibody preparations cross-react with
505 chalky and foliated extracts, suggesting partial overlaps in the protein compositions of these
506 two microstructures. Interestingly, the two GP bleeding batches gave the highest difference
507 between extracts of the chalky and of the foliated microstructures. We exploited these
508 differential *in vitro* responses to perform *in situ* immuno-histological localization on *C. gigas*
509 shell sections. The first antibody (SER323) marked predominantly, both on ELISA and on
510 histological preparations, the chalky layer, while the second antibody (SER324), when tested
511 with the similar techniques, marked the foliated layer, and some peculiar substructures of the
512 chalky one. To our knowledge, this is the first time that this property can be subtly exploited
513 for differential marking of shell microstructures. In former studies on nacro-prismatic
514 bivalves (Marin et al., 2000; Marie et al., 2012), we identified protein markers that were
515 present in one shell layer and absent in the adjacent layer.
516 How is the chalky layer synthesized and why is such a mechanically poor
517 microstructure produced in the shell of *C. gigas*? As underlined in the introduction, the chalky
518 layer typifies ostreid shell microstructures, although this peculiar microstructure is also
519 present in other bivalve groups such as the spondylids (Vermeij 2014). Structurally speaking,
520 the chalky layer consists of thin ‘bladelike structures oriented perpendicularly to the inner
521 shell surface’ (Vermeij 2014). This structure is hollow, extremely light, and discontinuous,

*i.e.*, exhibits a lenticular shape. According to the extensive review of Korringa (1951) on chalky deposits in the shell of *Ostrea edulis*, 'chalky layers are an economy building measure by the oyster (…) their function is to smooth out irregularities on the inside of the shell'. Further, Korringa defines chalky deposits as 'cheap padding'. Interestingly, this author calculated that chalky deposits allow to fill the space with 'one-fifth of the shell material that would be required if the folia layers were to be deposited'. Margolis and Carver (1974) consider that 'deposition of calcite in the form of chalky deposits occurs as a specific physiological response to environmental stimuli, possibly during periods of maximum respiration'. It has been suggested that the chalky deposit is a rapid filling layer in periods of high growth rates (Palmer and Carriker 1979). Recently, Chinzei (2013) suggested that the function of chalky deposits is to lighten the shell as an adaptation to soft substrates.

From a physiological and cellular viewpoint, it is unclear by which mechanism chalky deposits are secreted: Orton and Amirthalingam (1927) assumed that they are formed in the places where the mantle loses contact with the shell. According to Palmer and Carriker (1979), all the mantle epithelial cells capable of depositing foliated layers have the ability to also deposit the chalky ones. In a very recent paper, Vermeij (2014) proposes a radically novel view for chalky layer (mocret) deposition: this process would occur remotely from the mantle tissues, which, in other words, strongly suggests that the deposition process is poorly controlled by the mantle epithelium and that this remote calcification is enhanced by carbonate-precipitating sulfate-reducing bacteria, which would 'colonize and occupy spaces filled with a mixture of extrapallial fluid and seawater', both, rich in sulphate. If so, this suggests that the deposition of chalky materials is mostly induced by an organic matrix of bacterial origin, which, in other words, means a completely different matrix as the one used for foliated shell deposition.

546 However, carbon isotope measurements from foliated and chalky deposits of oyster
547 shells by Ullmann et al. (2010) tend to refute the influence of sulfate-reducing bacteria in the
548 oyster shell mineralization. Indeed, isotopic signatures are identical in both microstructures (-
549 1.11 ±0.64 ‰, n=83, and -1.02 ±0.32 ‰, n=100, for foliated and chalky layers, respectively)
550 while sulfate-reducing bacteria generally induce more negative values (around -10 ‰; Jia et
551 al. 2015).
552 Our immunogold staining of the shell of *C. gigas* does not allow a firm and definitive
553 conclusion on this matter. There is a clear differential immunogold marking of the two
554 microstructures, as shown by the immunogold results obtained with antibodies from rat
555 SER323. On the other hand, results obtained *in vitro* (ELISA) with chalky and foliated
556 extracts and immunogold staining with antibodies from rat SER324 suggest that part of the
557 epitopes of the chalky and of the foliated deposits are common to these two microstructures.
558 In particular, the locally-restricted marking of the chalky layers by SER324 antibodies is
559 limited to areas with a different aspect on those layers (Fig. 7e-h). These structures seem to
560 expand vertically all the way through the chalky layer (Fig. 7e). They may represent some
561 peculiar foliated structures that serve as “pillars” or “scaffolding” to help maintaining
562 integrity of the porous chalky layer. It has also been observed (de Rafélis, unpublished data)
563 that some micron-scale foliated layers were sometimes present in the chalky menisci of the
564 hinge region of the shell.
565 One important point concerns the temporal and geometrical continuity between the
566 foliated and chalky layers. Manganese labelling (Lartaud et al. 2010b) provided clear
567 evidence that the thin (5 micrometres thick) manganese-rich layer that is marked in the
568 foliated layer continues in the chalky one (see supplementary figure S2), although thickened
569 and more diffuse (Langlet et al. 2006; Lartaud 2007). This provides evidence that the two
570 microstructures are synthesized simultaneously, without temporal shift. We observed a similar

phenomenon, on a different mollusc model, the green ormer *Haliotis tuberculata* (Fleury et al. 2008). In shell repair experiments, we observed the formation of very different microstructures in continuity to one another, suggesting, first, an extraordinary plasticity of the functioning of the calcifying epithelium, and secondly, the possibility that the secretion of similar (or partly overlapping) matrix repertoires can generate very different microstructures. For chalky *versus* foliated microstructures, the question remains open.

**Compliance with ethical standards**

We declare that raising polyclonal antibodies from rats was performed according to ethical standards. We declare no conflict of interest.

**Acknowledgments**

The work presented in this paper was made possible by the ENS PhD programme. The Earth and Natural Sciences Doctoral Studies Programme is funded under the Programme for Research in Third-Level Institutions Cycle-5 and co-funded under the European Regional Development Fund. The entire experimental work was performed in Dijon, via a financial support attributed to V. M. by the Irish Geological Association and the AllTech Innovation Competition. The work of F. M. was supported by INTERRVIE Program (INSU, CNRS) and OSU-Theta. The final publication is available at Springer via http://link.springer.com/article/10.1007%2Fs00227-016-3040-6.

596 **References**

597 Addadi L, Joester D, Nudelman F, Weiner S (2006) Mollusk shell formation: A source of new
598 concepts for understanding biomineralization processes. Chem-Eur J 12: 980-987. doi:
599 10.1002/chem.200500980.
600 Ahr WM (2008) Geology of Carbonate Reservoirs. Wiley & Sons, Hoboken, New Jersey.
601 Albeck S, Aizenberg J, Addadi L, Weiner S (1993) Interactions of various skeletal
602 intracrystalline components with calcite crystals. J Am Chem Soc 115: 11691-11697. doi:
603 10.1021/ja00078a005.
604 Bougeois L, de Rafélis M, Reichart G-J, de Nooijer L.J., Nicollin F, Dupond-Nivet G (2014)
605 A high resolution study of trace elements and stable isotopes in oyster shells to estimate
606 Central Asian Middle Eocene seasonality. Chem Geol 363:200-212. doi:
607 10.1016/j.chemgeo.2013.10.037.
608 Bougeois L, de Rafélis M, Reichart G-J, de Nooijer LJ, Dupond-Nivet G (2016) Mg/Ca in
609 fossil oyster shells as palaeotemperature proxy, an example from the Palaeogene of Central
610 Asia. Palaeogeogr Palaeoclim Palaeoecol 441: 611-626. doi:10.1016/j.palaeo.2015.09.052.
611 Bricteux-Grégoire S, Duchâteau-Bosson G, Jeuniaux C, Florkin M (1964) Constituants
612 osmotiquement actifs des muscles adducteurs de *Gryphaea angulata* adaptée à l'eau de mer
613 ou à l'eau saumâtre. Arch Int Phys Bioch 72: 835-842.
614 Carter JG (1990) Evolutionary significance of shell microstructure in the Palaeotaxodonta,
615 Pteriomorphia and Isofilibranchia (Bivalvia: Mollusca). In: Carter JG (ed) Skeletal
616 Biomineralization: Patterns, Processes and Evolutionary Trends. Van Nostrand Reinhold,
617 New York, Chapter 10, pp 135-296.
618 Carter JG, Clark II GR (1985) Classification and phylogenetic significance of mollusk shell
619 microstructures. In: Broadhead TW (ed) Mollusk, Note for a Short Course, Studies in

Geology 13, Dpt. Of Geological Sciences. University of Tennessee Press, Tennessee pp 50-71.

Chinzei K (2013) Adaptation of oysters to life on soft substrates. Hist Biol 25: 223-231. doi: 10.1080/08912963.2012.727412.

Clark MF, Adams AN (1977) Characteristics of the microplate method of enzyme-linked immunosorbent assay for the detection of plant viruses. J Gen Virol 34: 475-483. doi: 10.1099/0022-1317-34-3-475.

Cranford S, Buehler MJ (2010) Materiomics: biological protein materials, from nano to macro. Nanotechnol Sci Appl 3: 127-148.

Fleury C, Marin F, Marie B, Luquet G, Thomas J, Josse C, Serpentini A, Lebel JM (2008) Shell repair process in the green ormer *Haliotis tuberculata*: a histological and microstructural study. Tissue Cell, 40: 207-218.

Gosling E (2003) Bivalve Molluscs: Biology, Ecology and Culture. Wiley-Blackwell, Oxford.

Hanly WC, Artwohl JE, Bennett BT (1995) Review of polyclonal antibody production procedures in mammals and poultry. ILAR J 37:93–118. doi: 10.1093/ilar.37.3.93.

Jia L, Cai C, Yang H, Li H, Wang T, Zhang B, Jiang L, Tao X (2015) Thermochemical and bacterial sulfate reduction in the Cambrian and Lower Ordovician carbonates in the Tazhong Area, Tarim Basin, NW China: evidence from fluid inclusions, C, S, and Sr isotopic data. Geofluids 15: 421-437. doi: 10.1111/gfl.12105.

Kanold JM, Immel F, Broussard C, Guichard N, Plasseraud L, Corneillat M, Alcaraz G, Brümmer F, Marin F (2015) The test skeletal matrix of the black sea urchin *Arbacia lixula*. Comp Biochem Physiol D 13: 24-34. doi: 10.1016/j.cbd.2014.12.002.

Korringa, P (1951) On the nature and function of “chalky” deposits in the shell of *Ostrea edulis* Linnaeus. Proc Calif Acad Sci 4th ser 27: 133-158.

644 Langlet D, Alunno-Bruscia M, de Rafélis M, Renard M, Roux M, Schein E, Buestel D (2006)
645 Experimental and natural cathodoluminescence in the shell of *Crassostrea gigas* from Thau
646 lagoon (France): ecological and environmental implications. Mar Ecol Prog Ser 317: 143-156.
647 doi: 10.3354/meps317143.
648 Lartaud F (2007) Les fluctuations haute fréquence de l'environnement au cours des temps
649 géologiques. Mise au point d'un modèle de référence actuel sur l'enregistrement des contrastes
650 saisonniers dans l'Atlantique nord. Ph.D. thesis, UPMC-Paris 06, Paris.
651 Lartaud F, Emmanuel L, de Rafélis M, Ropert M, Labourdette N, Richardson CA, Renard M,
652 (2010a). A latitudinal gradient of seasonal temperature variation recorded in oyster shells
653 from the coastal waters of France and The Netherlands. Facies, 56: 13-25. doi:
654 10.1007/s10347-009-0196-2.
655 Lartaud F, de Rafélis M, Ropert M, Emmanuel L, Geairon P, Renard M (2010b) Mn labelling
656 of living oysters: Artificial and natural cathodoluminescence analyses as a tool for age and
657 growth rate determination of *C. gigas* (Thunberg, 1793) shells. Aquaculture 300: 206-217.
658 doi: 10.1016/j.aquaculture.2009.12.018.
659 Le Roy N, Jackson DJ, Marie B, Ramos-Sylva P, Marin F (2014) The evolution of metazoan
660 α-carbonic anhydrases and their roles in calcium carbonate biomineralization. Front Zool 11:
661 75. doi: 10.1186/s12983-014-0075-8.
662 Lowenstam HA, Weiner S (1989) On Biomineralization. Oxford University Press, New-York,
663 324p.
664 Margolis SV, Carver, RE (1974) Microstructure of chalky deposits found in shells of the
665 oyster *Crassostrea virginica*. Nautilus 88: 62-65.
666 Marie B, Luquet G, Pais De Barros J-P, Guichard N, Morel S, Alcaraz G, Bollache L, Marin
667 F (2007) The shell matrix of the freshwater mussel *Unio pictorum* (Paleoheterodonta,

668 Unionoida) - Involvement of acidic polysaccharides from glycoproteins in nacre
669 mineralization. FEBS J 274: 2933-2945. doi: 10.1111/j.1742-4658.2007.05825.x.
670 Marie B, Marin F, Marie A, Bédouet L, Dubost L, Alcaraz, G, Milet C, Luquet G (2009)
671 Evolution of nacre: Biochemistry and proteomics of the shell organic matrix of the
672 cephalopod *Nautilus macromphalus*. ChemBioChem 10: 1495-1506. doi: 10.1002/c
673 bic.200900009.
674 Marie B, Le Roy N, Luquet G, Zanella-Cléon I, Becchi M, Marin F (2010) Proteomic analysis
675 of the acid-soluble nacre matrix of the bivalve *Unio pictorum*: Detection of novel carbonic
676 anhydrase and putative protease inhibitor proteins. ChemBioChem 11: 2138-2147. doi:
677 10.1002/cbic.201000276.
678 Marie B, Zanella-Cléon I, Guichard N, Becchi M, Marin F (2011) Novel proteins from the
679 calcifying shell matrix of the Pacific oyster *Crassostrea gigas*. Mar Biotechnol 13: 1159-
680 1168. doi: 10.1007/s10126-011-9379-2.
681 Marie B, Joubert C, Tayalé A, Zanella-Cléon I, Belliard C, Piquemal D, Cochennec-Loreau
682 N, Marin F, Gueguen Y, Montagnani C (2012) Different secretory repertoires control the
683 biomineralization processes of prisms and nacre deposition of the pearl oyster shell. Proc Natl
684 Acad Sci USA 109: 20986-20991.doi: 10.1073/pnas.1210552109.
685 Marin F (2003) Molluscan shell matrix characterization by preparative SDS-PAGE. Scientific
686 World J 3: 342-347. doi: 10.1100/tsw.2003.30.
687 Marin F, Gillibert M, Westbroek P, Muyzer G, Dauphin Y (1999) Evolution: Disjunct
688 degeneration of immunological determinants. Geol Mijnbouw 78: 135-139. doi:
689 10.1023/A:1003882928828.
690 Marin F, Corstjens P, De Gaulejac B, De Vrind-De Jong E, Westbroek P (2000) Mucins and
691 molluscan calcification: molecular characterization of mucoperlin, a novel acidic mucin-like

692 protein of the nacreous shell-layer of the fan mussel *Pinna nobilis* (Bivalvia, Pteriomorphia).
693 J Biol Chem 275: 20667-20675.doi: 10.1074/jbc.M003006200.
694 Marin F, Pereira L, Westbroek P (2001) Large-scale fractionation of molluscan shell matrix.
695 Protein Expres Purif 23: 175-179. doi: 10.1006/prep.2001.1487.
696 Marin F, Amons R, Guichard N, Stigter M, Hecker A, Luquet G, Layrolle P, Alcaraz G,
697 Riondet C, Westbroek P (2005) Caspartin and calprismin, two proteins of the shell calcitic
698 prisms of the Mediterranean fan mussel *Pinna nobilis*. J Biol Chem 280: 33895-33908. doi:
699 10.1074/jbc.M506526200.
700 Marin F, Le Roy N, Marie B (2012) The formation and mineralization of mollusk shell. Front
701 Biosci (Schol Ed) 4: 1099-1125.
702 Márquez-Aliaga A, Jiménez-Jiménez AP, Checa AG, Hagdorn H (2005) Early oysters and
703 their supposed Permian ancestors. Palaeogeogr Palaeoclim Palaeoecol 229: 127-136. doi:
704 10.1016/j.palaeo.2005.06.034.
705 Miyamoto H, Miyashita T, Okushima M, Nakano S, Morita T, Matsushiro A (1996) A
706 carbonic anhydrase from the nacreous layer in oyster pearls. Proc Natl Acad Sci 93: 9657-
707 9660.
708 Morrissey JH (1981) Silver stain for proteins in polyacrylamide gels: A modified procedure
709 with enhanced uniform sensitivity. Anal Biochem 117: 307-310. doi: 10.1016/0003-
710 2697(81)90783-1.
711 Mouchi V, de Rafélis M, Lartaud F, Fialin M, Verrecchia E (2013) Chemical labelling of
712 oyster shells used for time-calibrated high-resolution Mg/Ca ratios: A tool for estimation of
713 past seasonal temperature variations. Palaeogeogr Palaeoclim Palaeoecol 373: 66-74. doi:
714 10.1016/j.palaeo.2012.05.023.
715 Orr JC, Fabry VJ, Aumont O, Bopp L, Doney SC, Feely RA, Gnanadesikan A, Fruber N,
716 Ishida A, Joos F, Key RM, Lindsay K, Maier-Reimer E, Matear R, Monfray P, Mouchet A,

717 Najjar RG, Plattner G-K, Rodgers KB, Sabine CL, Sarmiento JL, Schlitzer R, Slater RD,
718 Totterdel IJ, Weirig M-F, Yamanaka Y, Yool A (2005) Anthropogenic ocean acidification
719 over the twenty-first century and its impact on calcifying organisms. Nature 437: 681-686.
720 doi: 10.1038/nature04095.
721 Orton JH, Amirthalingam, C (1927) Notes on Shell-Depositions in Oysters. J Mar Biol Assoc
722 UK 14: 935-954.
723 Osuna-Mascaró A, Cruz-Bustos T, Benhamada S, Guichard N, Marie B, Plasseraud L,
724 Corneillat M, Alcaraz G, Checa A, Marin F (2014) The shell organic matrix of the crossed
725 lamellar queen conch shell (*Strombus gigas*). Comp Biochem Physiol B 168: 76-85. doi:
726 10.1016/j.cbpb.2013.11.009.
727 Palmer RE, Carriker MR (1979) Chalky deposits in the shell of *Crassostrea virginica*:
728 Ultrastructure and environmental interactions. Proc Natl Shellfish Ass 69: 198-199.
729 Rhoads, DC, Lutz, RA eds (1980) Skeletal Growth of Aquatic Organisms: Biological.
730 Records of Environmental Change, Topics in Geobiology vol 1, Plenum Press, New-York.
731 Runnegar B (1984) Crystallography of the foliated calcite shell layers of bivalve molluscs.
732 Alcheringa 8: 273-290.
733 Samata T, Ikeda D, Kajikawa A, Sato H, Nogawa C, Yamada D, Yamazaki R, Akiyama T
734 (2008) A novel phosphorylated glycoprotein in the shell matrix of the oyster *Crassostrea*
735 *nippona*. FEBS J 275: 2977-2989. doi: 10.1111/j.1742-4658.2008.06453.x.
736 Shevchenko A, Loboda A, Werner E, Schraven B, Standing KG, Shevchenko A (2001)
737 Archived polyacrylamide gels as a resource for proteome characterization by mass
738 spectrometry. Electrophoresis 22: 1194-1203. doi: 10.1002/1522-2683()22:6<1194::AID-
739 ELPS1194>3.0.CO;2-A.
740 Simkiss K, Wilbur KM (1989) Biomineralization: Cell Biology and Mineral Deposition.
741 Academic Press, San Diego.

742 Taylor JD, Kennedy WJ, Hall A (1969) The shell structure and mineralogy of the Bivalvia.
743 Introduction. Nuculacea-Trigonacea. Bull Br Mus Nat Hist Zool Suppl 3: 1-125.
744 Thresh JM, Adams AN, Barbara DJ, Clark MF (1977) Detection of 3 viruses of Hop
745 (*Humulus lupulus*) by enzyme-linked immunosorbent assay (ELISA). Ann Appl Biol 87: 57-
746 65.
747 Towbin H, Staehelin T, Gordon J (1979) Electrophoretic transfer of proteins from
748 polyacrylamide gels to nitrocellulose sheets - procedure and some applications. Proc Natl
749 Acad Sci USA 76: 4350-4354.
750 Ullmann CV, Wiechert U, Korte C (2010) Oxygen isotope fluctuations in a modern North Sea
751 oyster (*Crassostrea gigas*) compared with annual variations in seawater temperature:
752 Implications for palaeoclimate studies. Chem Geol 277: 160-166. doi:
753 10.1016/j.chemgeo.2010.07.019.
754 Van Rooij D, De Mol L, Le Guilloux E, Wisshak M, Huvenne VAI, Moeremans R, Henriet J-
755 P (2010) Environmental setting of deep-water oysters in the Bay of Biscay. Deep-Sea Res I
756 Oceanogr Res Pap 57: 1561-1572. doi: 10.1016/j.dsr.2010.09.002.
757 Vermeij GJ (2014) The oyster enigma variations: A hypothesis of microbial calcification.
758 Paleobiology 40: 1-13. doi: 10.1666/13002.
759 Weiner S, Traub W (1984) Macromolecules in mollusc shells and their functions in
760 biomineralization. Phil Trans R Soc Lond B 304: 425-434. doi: 10.1098/rstb.1984.0036.
761 Zhang G, Fang X, Guo X, Li L, Luo R, Xu F, Yang P, Zhang L, Wang X, Qi H et al (2012)
762 The oyster genome reveals stress adaptation and complexity of shell formation. Nature 490:
763 49-54.
764

Table 1: summary of the LC-MS/MS analysis of the purified F21-22 fraction of the shell matrix of *C. gigas*. a: accession number of each protein hit according to NCBI database ; b: protein name according to NCBI database ; MW: theoretical molecular weight in Daltons, calculated from the identified protein (in parentheses, AA nb = number of amino acid residues); c: list of peptides identified by the analysis.

| Accession number[a] | Protein identification[b] | Species | MW (AA nb) | Protein score | MS/MS peptides[c] | Peptide score |
|---|---|---|---|---|---|---|
| gi\|317376184\| | Gigasin-6 | *Crassostrea gigas* | 34106 (302) | 65 | R.STIQEVYK.N<br>K.NPGVIVSVVK.D<br>K.NEIYTPLGMAK.S | 35<br>8<br>21/(18)/(12) |
| gi\|762132907\| | Gigasin-6 isoform X1 | *Crassostrea gigas* | 62490 (552 ) | 65 | Same peptides as for Gigasin-6 | |
| gi\|762132909\| | Gigasin-6 isoform X2 | *Crassostrea gigas* | 61546 (543) | 65 | Same peptides as for Gigasin-6 | |
| gi\|762104436\| | Nacrein-likeprotein | *Crassostrea gigas* | 51244 (441) | 63 | K.TLSCLMEK.Y<br>K.KPSDYFIK.N<br>R.VEDTDNNPLK.E | 12<br>9<br>42 |
| gi\|512134004\| | Nacrein-likeprotein | *Crassostrea gigas* | 48258 (413) | 58 | K.TLSCLMEK.Y<br>K.KPSDYFIK.E<br>R.VEDTENNPLK.E | 12<br>9<br>36/(18)/(9) |
| gi\|762164175\| | Cell death abnormality protein 1-like | *Crassostrea gigas* | 28195 (255) | 56 | R.SDFECPR.D<br>R.AAGSISGGDPATGTEAADTGSGM.- | |

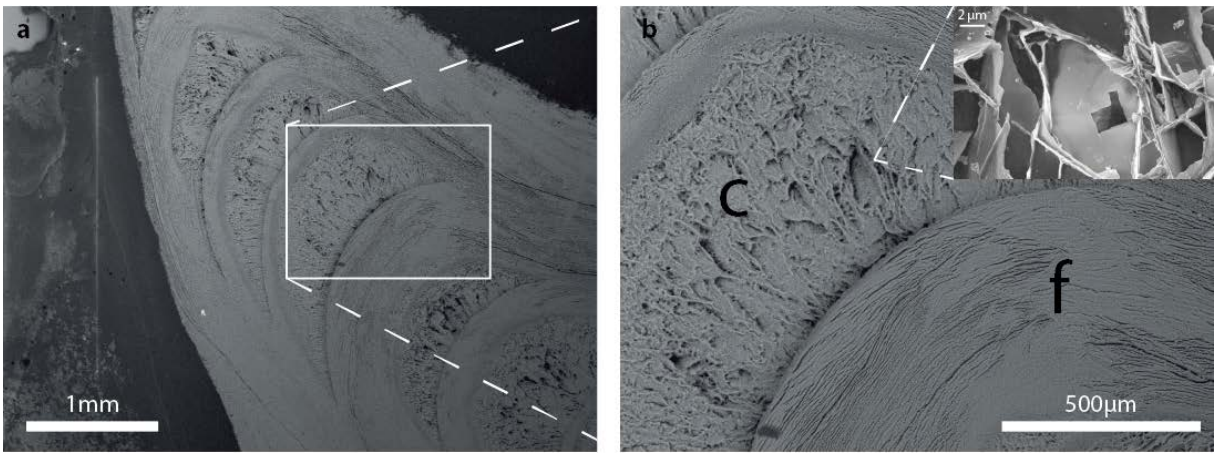


Figure 1: Microstructures in the umbo region of a *C. gigas* shell, longitudinal section, crossing the middle of the hinge region (perpendicular to the opening plan of the valves). **a:** Growth direction is from top left to bottom right. **b:** Detailed view (white square from a). "c" indicates the chalky structure while "f" corresponds to the foliated layers.

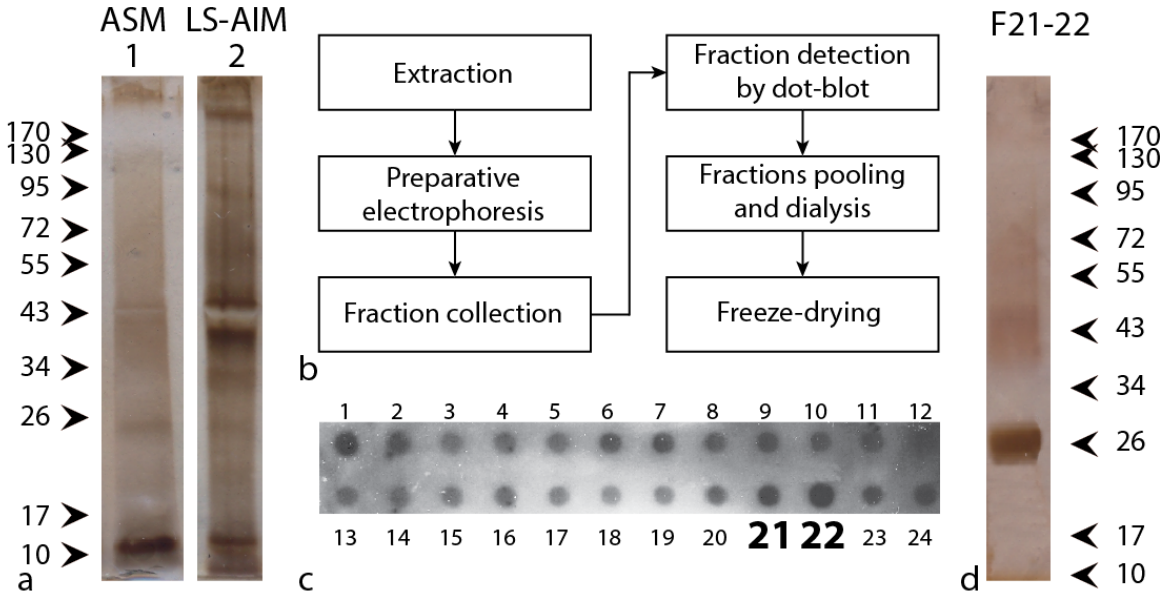


Figure 2: Characterization on monodimensional gels of the shell matrix of *C. gigas* and purification of one fraction. **a:** silver-stained gel electrophoresis of the acid-soluble (ASM, lane 1) and of the Laemmli-soluble acid-insoluble (LS-AIM, lane 2) matrices. Markers of different molecular weight (in kDa) are indicated on the left. **b:** Summary of the protocol used from the extraction to the freeze-drying of the purified fraction. **c:** dot-blot (performed after preparative electrophoresis) showing the cross-reactivities of the different fractions with anti-caspartin antibody (see text). Only the 24 first fractions are illustrated here. Note that the fractions of tubes 21 and 22 (F21-22) give the strongest signal. **d:** Gel electrophoresis of the F21-22 fraction, showing the apparent purity of this fraction, which was subsequently used for eliciting polyclonal antibodies. Markers of different molecular weight (in kDa) are indicated on the right.

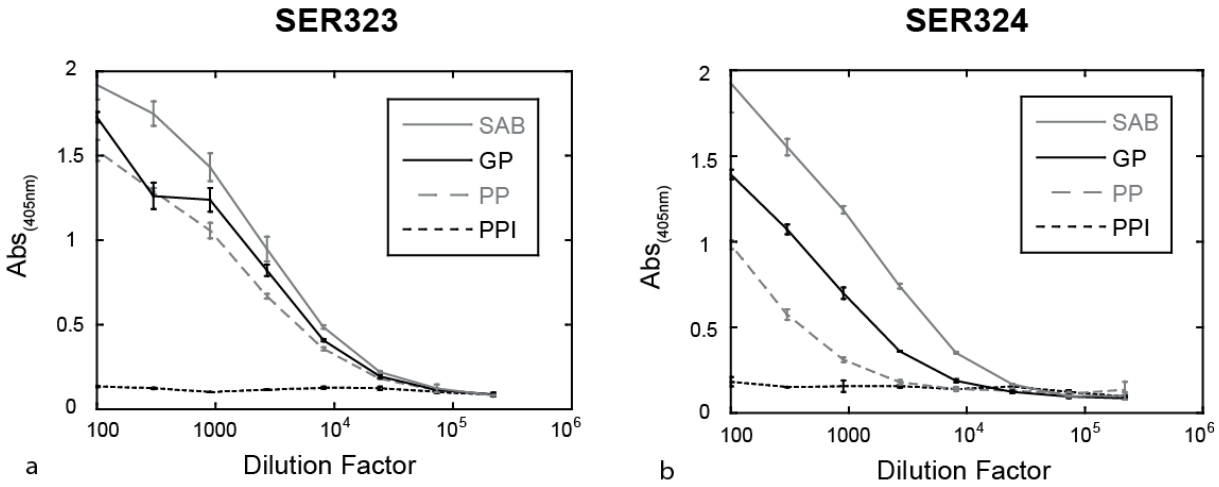


Figure 3: Titers of the ELISA tests performed on the antibodies produced by SER323 (**a**) and SER324 (**b**). PPI: pre-immune bleed. PP: small bleed. GP: large bleed. SAB: final bleed. Note that the two rats behave differently to the repetitive injections.

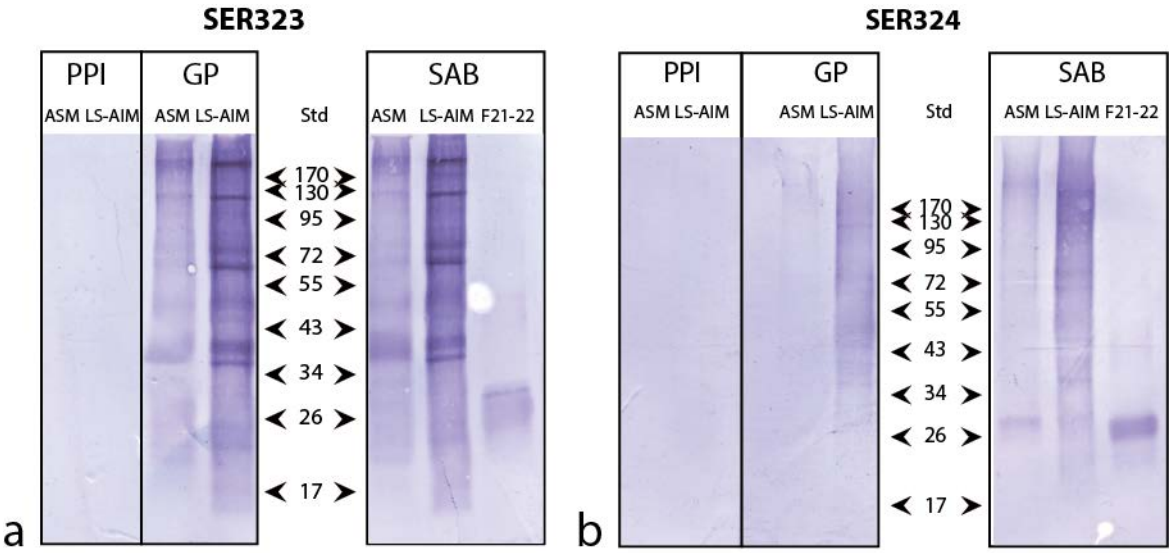


Figure 4: Western-blots of the ASM, LS-AIM and F21-22 fraction with polyclonal antibodies elicited against the F21-22 fraction. The PPI, GP and SAB antisera, produced in rat SER323 (**a**) and rat SER324 (**b**) were tested. Std: markers standard; the corresponding molecular weights (in kDa) are indicated on the right.

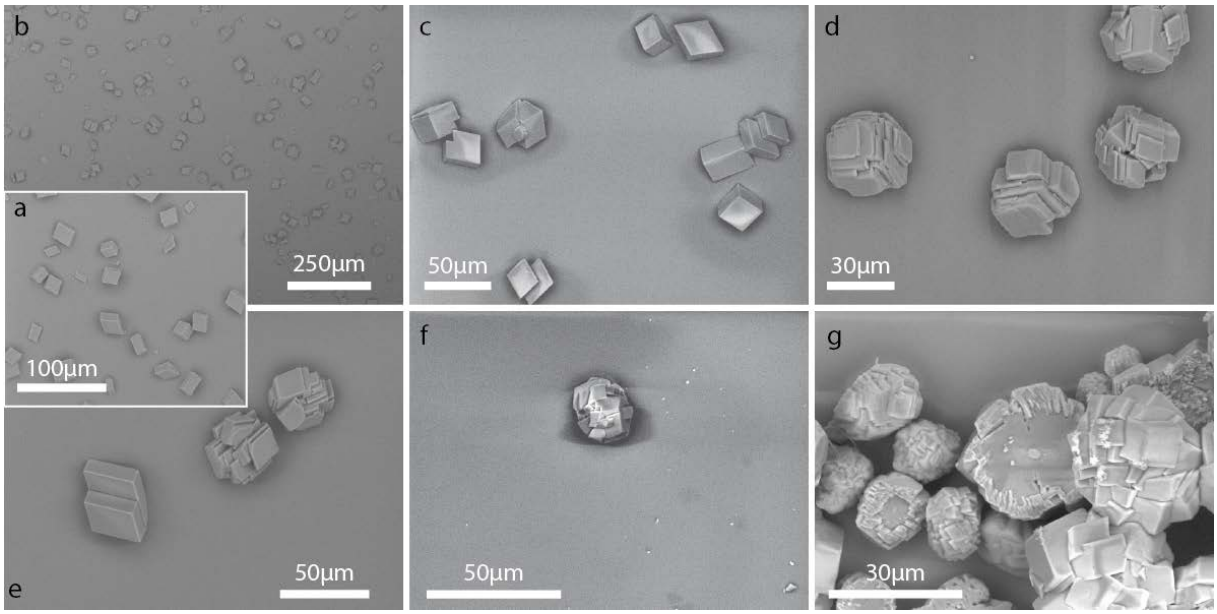

Figure 5: *In vitro* crystallization of calcium carbonate at different concentrations of F21-22 (**b-d**) and of ASM (**e-g**). **a**: 0 µg/mL.**b, e**: 0.3125 µg/mL.**c, f**: 5 µg/mL.**d, g**: 20 µg/mL.

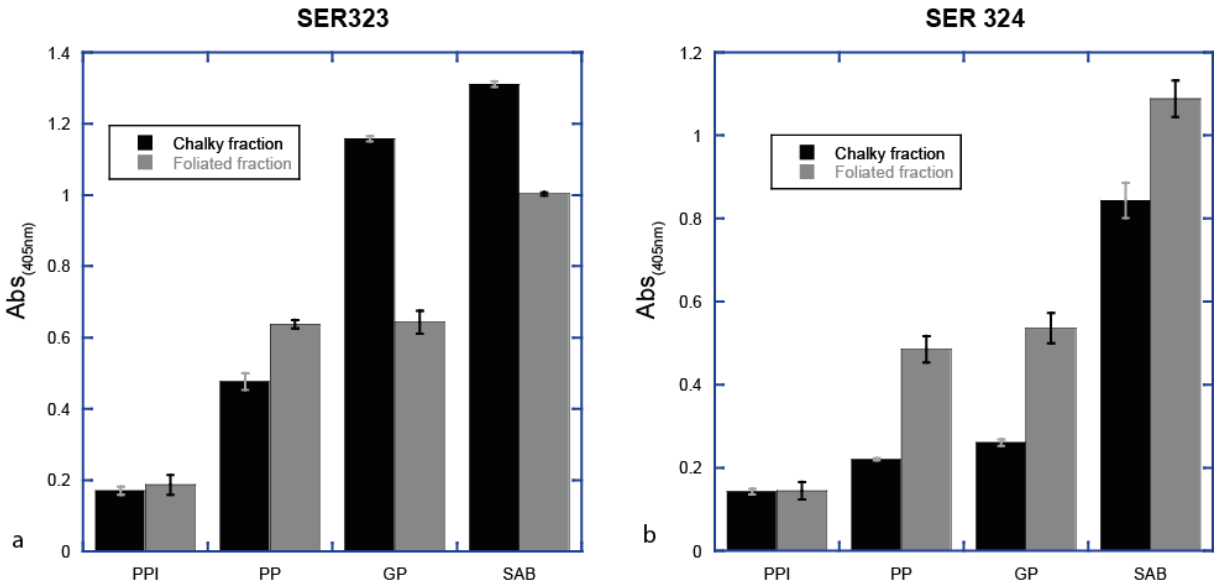

Figure 6: Differences in ELISA tests on chalky and foliated fractions with antibodies produced by SER323 (**a**) and SER324 (**b**) rats. Abs: absorbance, arbitrary units. PPI: pre-immune bleed. PP: small bleed. GP: large bleed. SAB: final bleed.

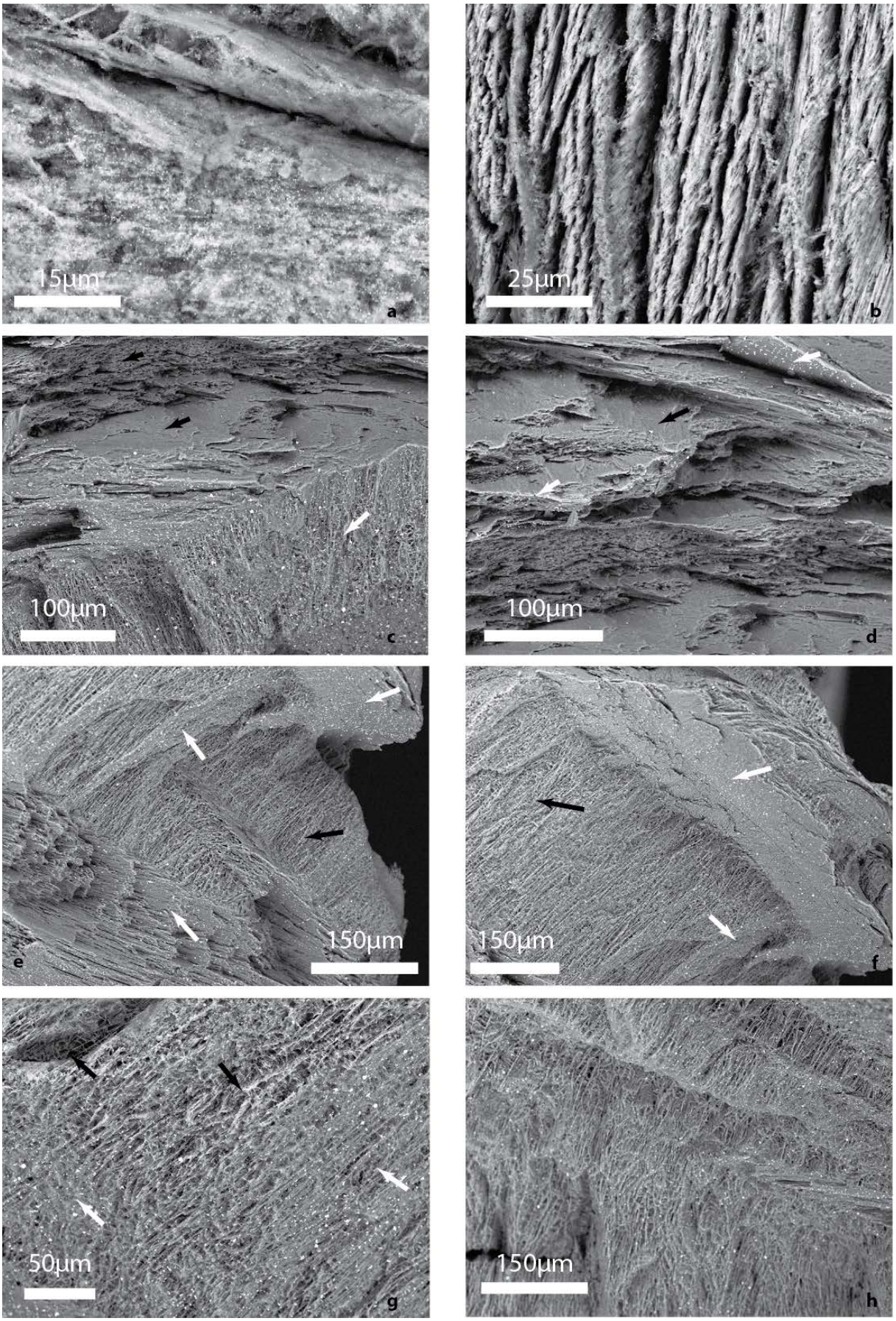

Figure 7: Immunogoldlocalization using the polyclonal antibodies raised against the F21-22 fraction on *C. gigas* shell. For evidencing the differential staining - according to the results of

Fig. 6 - we used GP antibodies produced by SER323 and SER324. **a-b:** Thin sections treated with SER323 antibodies. **c-d:** Fresh fractures treated with SER323 antibodies. **e-h:** Fresh fractures treated with SER324 antibodies. White arrows indicate positive immunolocalization while black arrows point to areas with no staining. For SER323 (**a-d**) only the chalky layers are stained. It is the opposite for SER324 (**e-h**) as the foliated areas are stained. Only specific areas of the chalky deposits, standing out from the rest of these structures, are stained by SER324.